Contrib Mineral Petrol (2009) 158:703–722
DOI 10.1007/s00410-009-0406-5

ORIGINAL PAPER

Protracted fluid-induced melting during Barrovian metamorphism in the Central Alps

Daniela Rubatto · Jörg Hermann · Alfons Berger · Martin Engi

Received: 22 December 2008 / Accepted: 14 April 2009 / Published online: 2 May 2009

Abstract The timing and dynamics of fluid-induced melting in the typical Barrovian sequence of the Central Alps has been investigated using zircon chronology and trace element composition. Multiple zircon domains in leucosomes and country rocks yield U–Pb ages spanning from ~32 to 22 Ma. The zircon formed during Alpine melting can be distinguished from the inherited and detrital cores on the basis of their age, Th/U (<0.1) and trace element composition. Ti-in-zircon thermometry indicates crystallization temperatures around 620–700°C. Their composition allows discriminating between (1) zircon formation in the presence of early garnet, (2) zircon in equilibrium with abundant L-MREE-rich accessory phases (allanite, titanite and apatite) typical of metatonalites, and (3) zircon formed during melting of metasediments in feldspar-dominated assemblages. The distribution of zircon overgrowths and ages indicate that repeated melting events occurred within a single Barrovian metamorphic cycle at roughly constant temperature; that in the country rocks zircon formation was limited to the initial stages of melting, whereas further melting concentrated in the segregated leucosomes; that melting occurred at different times in samples a few meters apart because of the local rock composition and localized influx of the fluids; and that leucosomes were repeatedly melted when fluids became available. The geochronological data force a revision of the temperature–time path of the migmatite belt in the Central Alps. Protracted melting over 10 My followed the fast exhumation of Alpine eclogites contained within the same region and preceded fast cooling in the order of 100°C/Ma to upper crustal levels.

Communicated by J. Hoefs.

Electronic supplementary material The online version of this article (doi:10.1007/s00410-009-0406-5) contains supplementary material, which is available to authorized users.

D. Rubatto (✉) · J. Hermann
Research School of Earth Sciences, The Australian National University, Canberra, ACT 0200, Australia
e-mail: Daniela.rubatto@anu.edu.au

A. Berger · M. Engi
Institute of Geological Sciences, University of Bern, Baltzerstrasse 1-3, 3012 Bern, Switzerland

A. Berger
Institute for Geography and Geology, Øster Voldgade 10, 1350 Copenhagen, Denmark

Introduction

Partial melting is the principal geological process for the formation and fractionation of the continental crust. It is also relevant for the rheological behaviour of the crust, particularly during collisional orogenies (e.g. Faccenda et al. 2008). Within the crust, melting may be triggered by an externally derived fluid (mainly H_2O-rich) via fluid-induced melting (e.g. Prince et al. 2001), or during dehydration reactions involving a hydrous phase (hydrate-breakdown melting) such as muscovite, biotite or amphibole (Le Breton and Thompson 1988). The latter process is by far the best documented in anatectic terranes, and can produce large melt fractions and ultimately granitic bodies (Clemens and Vielzeuf 1987). Fluid-induced melting generally occurs at lower temperatures, during the prograde path and requires an external fluid source. Melt production during hydrate-breakdown melting is controlled by temperature (T), pressure (P) and the amount of hydrous phases and can thus be modelled (White et al. 2007). On

the other hand, water assisted melting is controlled by the external fluid source (Berger et al. 2008) and thus it is difficult to predict, quantify and model.

Crustal melting is best constrained in time using U–Pb dating of zircon and monazite, which readily crystallize in a melt when saturation of Zr and LREE is reached. Models predict that, during hydrate-breakdown melting, accessory zircon and monazite will mainly form at the metamorphic peak and/or during decompression (Kelsey et al. 2008). Geochronological investigations of migmatites in granulite-facies terranes that underwent prevalently hydrate-breakdown melting indicate that zircon and monazite (re-) crystallization in the presence of melt can extend over several million years up to 20–30 My (e.g. Williams et al. 1996; Kalt et al. 2000; Jung and Mezger 2001; Rubatto et al. 2001; Hermann and Rubatto 2003; Montero et al. 2004). In these regional metamorphic settings, rocks of different compositions can melt at different times during the *P–T* path and, if the temperature remains high, melting can be protracted over a long period.

During fluid-induced melting, melt will form and readily crystallize at any time when the H_2O-rich fluid is consumed, partly independently of how the rock evolves in *P–T*. In principle, introduction of fluids will produce a short-lived melting event, which can potentially repeat each time fluids enter the system. There is however little geochronological information on the duration and episodic or continuous nature of such melting, largely because few terranes have been studied, in which fluid-induced melting is dominant. One main reason for this is that in many terranes initial fluid-induced melting is generally overprinted by higher grade hydrate-breakdown melting, making it difficult to exactly time the duration of fluid-induced melting.

The migmatites of the Central Alps have been documented as a major terrane dominated by fluid-induced melting, which was not obliterated by later hydrate-breakdown melting (Burri et al. 2005; Berger et al. 2008). The migmatites comprise a variety of protoliths (granitoids and sediments), which contain multiple generations of variably deformed leucosomes. The distribution of leucosome is heterogeneous and spatially variable at the outcrop scale, even when hosted in a homogeneous protolith (Burri et al. 2005; Berger et al. 2008). The extensive and variably distributed melting makes the migmatites of the Central Alps an ideal terrane where the temporal duration of melting can be investigated. Moreover, the relatively young age of the Alpine migmatites permits resolution of relatively short-lived melting events.

The Central Alps are also one of the classical localities for Barrovian-type metamorphism and arguably the most intensively studied from a geochronological point of view. Here the pioneers of the Rb–Sr and K–Ar system first applied these techniques to regional cooling after amphibolite-facies metamorphism (Steiger 1964; Hunziker 1969; Jäger 1973; Hurford 1986) and defined a monotonic cooling from Rb–Sr mica closure temperature ($\sim$500°C) to zircon fission tracks ($\sim$240°C) between 25 and 19 Ma (see a review in Hunziker et al. 1992). However, there is surprisingly little data on the age of peak metamorphism, and nothing about its duration. Fluid-assisted melting occurs at temperatures above the closure temperature for Rb–Sr and K–Ar, and thus requires more robust chronometers such as U–Pb. It has long been accepted that peak metamorphism and anatexis in the southernmost parts of the Central Alps occurred at around 30 Ma ($\pm$2 Ma) on the basis of few U–Pb and Sm–Nd ages (Köppel and Grünenfelder 1975; Vance and O'Nions 1992; Gebauer 1996; Romer et al. 1996; Schärer et al. 1996).

We present a systematic investigation of the timing of melting in the migmatites of the Central Alps using zircon U–Pb geochronology that challenges these current ideas on time and duration of Alpine anatexis. The new age data permit to constrain when and for how long fluid-induced melting occured. We also aim to resolve if melting was episodic or continuous and if different rock types recorded distinct portions of the metamorphic evolution. The challenging task of linking ages of U–Pb accessory minerals to metamorphic conditions is accomplished through petrology and zircon internal structure, thermometry and trace element composition.

Geological background

The Central Alps are a section of the Alpine chain in the southern part of Switzerland and in northern Italy that underwent Barrovian-type metamorphism during the Cenozoic following collision of Africa with Europe. In the area, metamorphism increases towards the south and is truncated by the Insubric line (Fig. 1), a major tectonic line that separates the Central Alps from the Southern Alps, where only weak Cenozoic metamorphism is recorded. This geometry derives from the subduction of the European plate in the north under the Apulian plate in the south, and the subsequent uplift of the lithosphere during continental collision (e.g. Steck and Hunziker 1994). Collision and exhumation are reflected by a sequence of deformation events (e.g. Schmid et al. 1996; Maxelon and Mancktelow 2005). Just north of the Insubric line is the intensely deformed region of the Southern Steep Belt (SSB), where peak metamorphism and extensive melting in amphibolite facies conditions are recorded (migmatite belt, see a summary of *P–T* conditions in Engi et al. 1995; Burri et al. 2005). The area consists of a tectonic mélange unit (Engi et al. 2001) containing basement fragments, which underwent Variscan

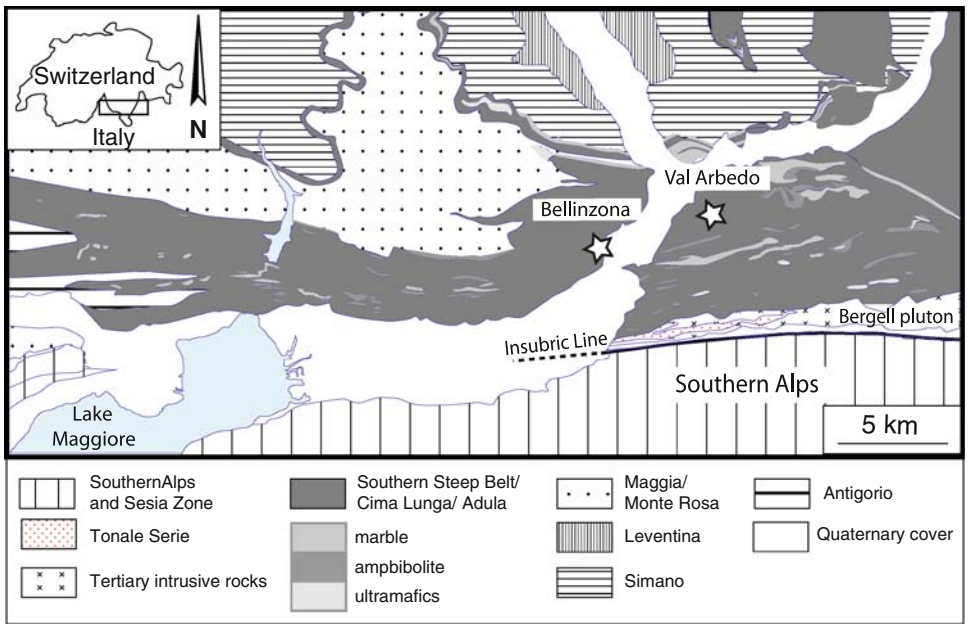

Fig. 1 Schematic geological map of the Southern Steep Belt with the two sample locations. After Berger et al. (2005)

(~300 Ma) high-grade metamorphism, as well as late Variscan granitoids (280–300 Ma), in addition to a variety of metasediments, mafic and ultramafic rocks, most of them polymetamorphic, but all finally affected by Alpine metamorphism. In the field, metamorphic conditions are thus complicated by intense deformation and mixing at the outcrop scale of Alpine and pre-Alpine high-grade rocks. This complexity created problems for geochronology, such as age inheritance in accessory minerals and difficulty in isolating Alpine ages (Romer et al. 1996). The migmatite zone contains variably deformed pegmatite and aplitic dikes, small granitic bodies (metre to decametre in size) as well as in situ migmatites (e.g. Burri et al. 2005).

The migmatite area and the amphibolite-facies rocks in the northern part of the Southern Steep Belt also contain abundant high-pressure relicts that testify for Alpine high pressure metamorphism as late as ~35 Ma (Gebauer 1996; Brouwer et al. 2005), before the onset of Barrovian metamorphism. Rapid exhumation of such eclogites to amphibolite facies conditions from ~35 to 33 Ma has been documented in a number of localities (Gebauer 1996; Hermann et al. 2006). Migmatisation of the eclogite country rocks has been dated at ~32 Ma (Gebauer 1996), preceding the 32–28 Ma crystallization of the largest pluton in the Southern Steep Belt, the Bergell pluton (von Blanckenburg 1992; Oberli et al. 2004).

Methods

Zircons were prepared as mineral separates mounted in epoxy and polished down to expose the grain centres. Cathodoluminescence (CL) imaging was carried out at the Electron Microscope Unit, Australian National University with a HITACHI S2250-N scanning electron microscope working at 15 kV, ~60 μA and ~20 mm working distance.

U–Pb analyses were performed using a sensitive, high-resolution ion microprobe (SHRIMP II) at the Research School of Earth Sciences. Instrumental conditions and data acquisition were generally as described by Williams (1998). The data were collected in sets of six scans throughout the masses. The measured $^{206}Pb/^{238}U$ ratio was corrected using reference zircon (Temora, 417 Ma, Black et al. 2003). Data were corrected for common Pb on the basis of the measured $^{207}Pb/^{206}Pb$ ratios and assuming concordance, as described in Williams (1998). Age calculation was done using the software Isoplot/Ex (Ludwig 2003) and assuming the common Pb composition predicted by Stacey and Kramers (1975). U–Pb data were collected over a number of analytical sessions using the same ion microprobe and standard, with different analytical sessions having calibration errors between 1.0 and 2.8% (2 sigma). Average ages are quoted at 95% confidence level (c.l.).

Trace element analyses of zircon were performed on the grain mount with a Laser Ablation–ICP-MS at the Research School of Earth Sciences, Canberra, using a pulsed 193 nm ArF Excimer laser with 100 mJ energy at a repetition rate of 5 Hz (Eggins et al. 1998) coupled to an Agilent 7500 quadrupole ICP-MS. A spot size of 24, 32 or 40 μm was used according to the dimension of the growth zone of interest. External calibration was performed relative to NIST 612 glass and internal standardisation was based on stoichiometry silica. Accuracy of the analyses was evaluated with a BCR-2G secondary glass standard and is always better than 15%. During the time-resolved

analysis of minerals, contamination resulting from inclusions, fractures and zones of different composition was monitored by several elements and only the relevant part of the signal was integrated.

Sample description

A series of leucosome (suffix "L") and associated country rock (suffix "M" for mesosome) pairs were sampled in two well studied key localities within the migmatite zone of the Southern Steep Belt (Burri et al. 2005; Berger et al. 2008). Country rocks are derived from either a tonalitic or sedimentary protolith and thus are distinguished as metatonalites and metasediments.

Val Arbedo (VA) is a steep valley 5 km N–NE of the city of Bellinzona. Samples were collected along a road cut that intersects the sequence across strike. Field relations are represented in Fig. 2. The three leucosome–country rock pairs investigated for geochronology (VAL1–VAM1, VAL2–VAM2 and VAL4–VAM4) are similar in mineral assemblage, with variable proportions of plagioclase, quartz, amphibole and biotite (Table 1), whereas K-feldspar is absent or very minor. A significant difference is the presence of relic garnet in metasediment VAM4, with traces of corroded garnet in leucosome VAL4.

VAM1 (Fig. 2a) is a weakly foliated, biotite-bearing amphibolite (green amphibole) deriving from a tonalite. It is rich in titanite, allanite and apatite as accessory phases. The portion of sample VAM1 used for zircon separation does not contain any cross cutting leucosome, but only thin layer-parallel leucosomes. The foliation in VAM1 is cut at low angle by leucosome VAL1 (Fig. 2a, b), which is openly folded and shows a weak foliation. It contains large green amphibole and scarce biotite.

VAM2 is a foliated metatonalite rich in biotite, which is crosscut by a coarse grained leucosome (VAL2) with large amphiboles and poor in accessory titanite and allanite, but containing abundant zircon. VAL1 and VAL2 are structurally young leucosomes that are discordant to the main foliation. In the same area deformed leucosomes also occur, which are either boudinaged or tightly folded.

Metasediment VAM4 has a significantly different composition with green-brown amphibole, biotite and scarce garnet. Garnet grains appear resorbed (rounded shape) and are intimately associated with biotite and amphibole. Accessory titanite, allanite, apatite and zircon are abundant. The rock contains anastomosing, small (<1 cm) leucosomes. The amphibolite is crosscut at high angle by a large (20–30 cm thick) leucosome dike VAL4 (Fig. 2c) that elsewhere is parallel to the foliation. The leucosome sample contains scarce biotite and is poor in accessory minerals. The contact between amphibolite and leucosome is marked by enrichment in biotite.

The outcrop at the locality near Bellinzona (BE, Fig. 2d) is along the local road between Carasso and Gorduno, NW of the city. It consists of intensely folded biotite-bearing migmatites with distinct leucosomes at various scales, from mm to dm, showing different degrees of deformation (Fig. 2d). Sample BEM1 is a banded biotite-rich migmatite with mm-size quartzo-feldspatic levels parallel to the foliation (Table 1). It is rich in allanite and apatite. It is difficult to establish the protolith of this sample from the field relations and assemblage, but the presence of ~280 Ma magmatic allanite (Gregory 2008) indicates it was a magmatic rock, most likely a tonalite or granodiorite. BEL1 forms a dm-sized leucosome along the axial plane of isoclinal-folds within the migmatite. It has a weak foliation marked by brown biotite and contains rare green amphibole and abundant accessory allanite, apatite and zircon.

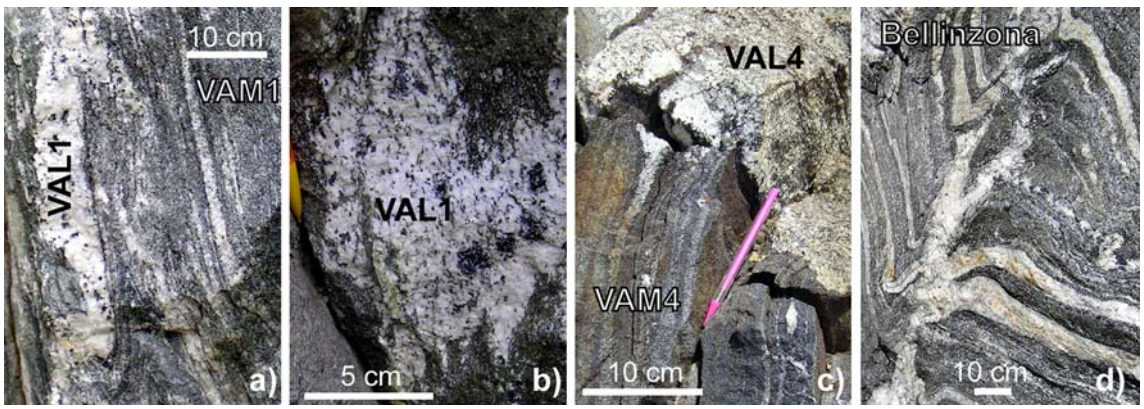

Fig. 2 Field occurrence of migmatites in the SSB. **a** Val Arbedo migmatite composed of a deformed leucosome (sample VAL1) and a country rock with thin, layer-parallel leucosomes (sample VAM1). **b** Detail of leucosome VAL1, note the large, poikilitic amphibole grains, and the weak foliation. **c** Metasedimentary banded amphibolite (sample VAM4) crosscut by coarse grained, large leucosome (VAL4). Note the sharp contact between amphibolite and leucosome. **d** Typical outcrop appearance of migmatites in the locality of Bellinzona. Note the different generations of variably deformed leucosome, crosscutting one another

Table 1 Summary of mineral assemblages, and zircon ages, Th/U compositions and temperatures in the investigated samples

Sample and rock type	Swiss grid coordinates	Assemblage	Zircon core age and Th/U	Alpine overgrowths age and Th/U	Temp[b] (°C)
VAM1	725,100	Amp Qtz Pl Bt ± Kfs	290–238 Ma	None	
Metatonalite	119,350	Tnt All Ap Zrn Mag	Th/U 0.2–6		
VAL1	725,100	Qtz Pl Bt Amp ± Kfs	290–274 Ma	22.12 ± 0.25 Ma, MSWD 0.94, N 12/12	630–670
Leucosome	119,350	All Zrn Tnt Mag	Th/U 0.1–9	Th/U 0.007–14	
VAM2	725,100	Pl Qtz Bt Amp ± Kfs	303–274 Ma	32.9–27.6 Ma (31.2 ± 2.5 MSWD 2.4, N 6/6)[a]	<700
Metatonalite	119,350	Tnt All Zrn	Th/U 0.2–4	Th/U 0.01–5	
VAL2	725,100	Pl Qtz Amp Bt ± Kfs	515, 299–246 Ma	31.9–22.6 Ma (23.1 ± 0.3 Ma, MSWD 3.6, N 8/22 and 27.4 ± 0.3 Ma MSWD 0.94, N 6/22)[a]	630–680
Leucosome	119,350	Zrn ± All	(294 ± 4, MSWD 4)		
			Th/U 0.1–7	Th/U 0.002–6	
VAM4	726,800	Pl Qtz Amp Bt Kfs Grt	584 and 483 Ma	48, 43 and 32 Ma	650–730
Metasediment	118,600	Tnt All Ilm Ap Zrn	Th/U 0.01 and 0.9	Th/U 0.02–6	
VAL4	726,800	Pl Qtz Kfs Bt ± Grt	2800–509 Ma	Ov1 30.8 ± 0.3 Ma, MSWD 2.5, N 18/18, Th/U 0.01	660–730
Leucosome	118,600	Ilm Zrn	Th/U 0.2–7	Ov2 26.1–29.6 Ma (28.4 ± 0.7 MSWD 4.3, N 10/11)[a], Th/U 0.01–2	650–690
BEL1	722,500	Pl Qtz Bt ± Kfs ± Amp	718, 596 and 304 Ma	Ov1 31.3 ± 0.3 Ma, MSWD 1.5, N 7/7, Th/U 0.002	650–670
Metasediment	118,700	All Ap Zrn Opac	Th/U > 0.1	Ov2 26.0 ± 0.3 Ma, MSWD 1.7, N 14/15 Th/U 0.002–6	620–640
				Ov3 23.3 ± 0.2 Ma, MSWD 2.1, N 14/14, Th/U 0.002–6	610–660
BEM1	722,500	PL Qtz Bt ± Kfs	311 Ma	32.0–23.7, 31.4 ± 0.3 Ma MSWD 0.94, N 9/12	640–690
Leucosome	118,700	All Ap Zrn	Th/U 0.9	Th/U 0.001–6	

[a] Best mean age of scattering analyses possibly indicating continuous growth. See *type 2* ages in text

[b] Temperature according to Ti-in-rutile thermometry of Watson and Harrison 2005, corrected for $a_{TiO2} = 0.5$

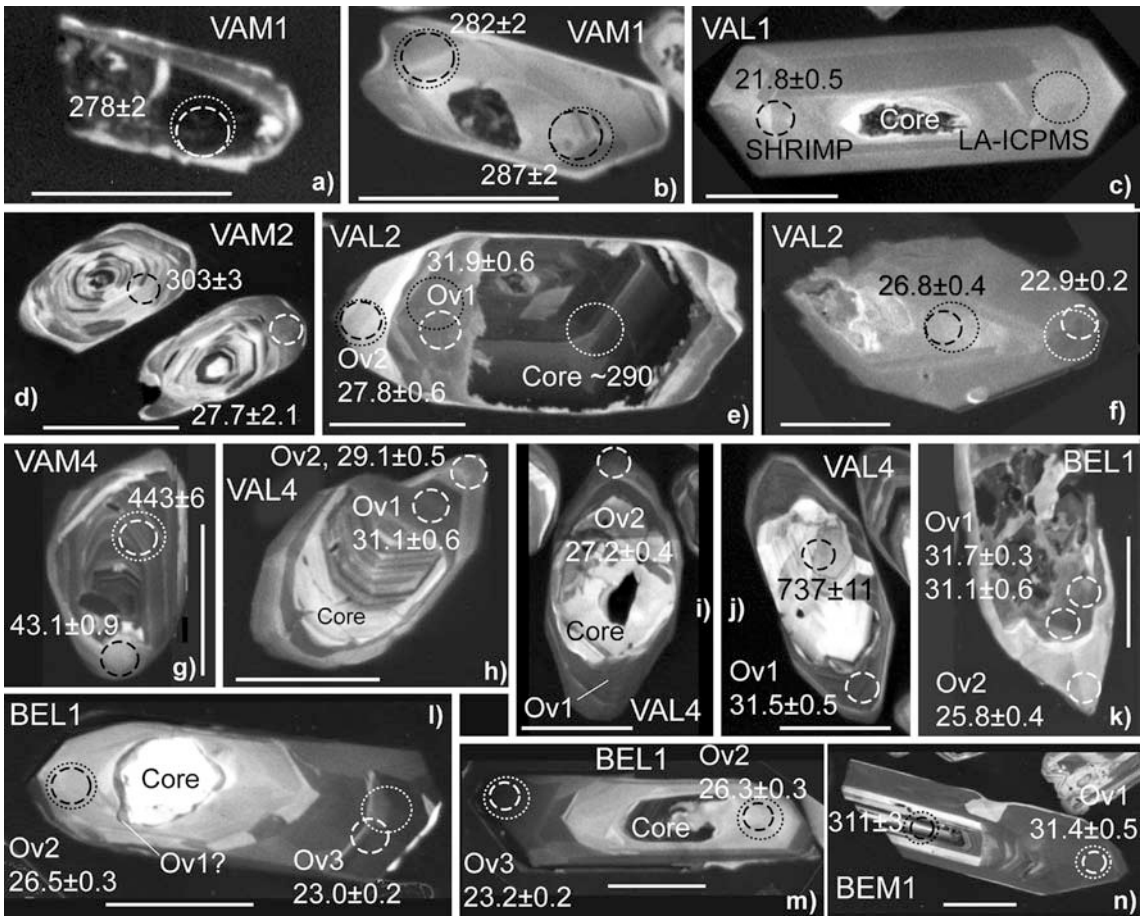

Fig. 3 Cathodoluminescence images of dated zircon crystals. *Dashed circles* indicate the location of SHRIMP U–Pb analyses; *dotted circles* the location of LA-ICPMS trace element analysis. The *white scale bar* in each image represents 100 μm. Ages for SHRIMP analyses are reported in Ma ± 1 sigma. **a** Zircon in VAM1 amphibolite with a dark Variscan core partly metamict (see mosaic zoning) surrounded by a thin rim. **b** Zircon from VAM1 amphibolite with a large rim surrounding the dark core. Note that the age of zircon rims in this sample is Variscan and not Alpine, despite the similarity with Alpine rims (see **c**). **c** Zircon in VAL1 leucosome with resorbed inherited core and large, euhedral anatectic overgrowth of alpine age. **d** Two zircon crystals from amphibolite VAM2, which largely consist of inherited cores and show only thin, unzoned metamorphic rims. **e** Zircon from leucosome VAL2 with two successive rims distinct in chemistry and age. The core was not dated, but is similar to other inherited cores in this sample that yield a ~290 Ma age. **f** Zircon in leucosome VAL2 with an apparent, progressive age decrease from core to rim within an apparently continuous growth zone. The inherited core is just exposed in the left corner of the crystal. **g** Zircon from amphibolite VAM4 with a large detrital core and a thin, unzoned Alpine rim. In this sample the few rims preserved yielded scattering ages, which are not considered geologically significant. **h** Zircon from leucosome VAL4 with two successive rims distinct in chemistry and age on a partly rounded detrital core. **i** Zircon from leucosome VAL4 with two distinct overgrowths. **j** Zircon from leucosome VAL4 with a well-developed internal overgrowth Ov1, and a thin, CL-brighter Ov2. **k** Zircon from leucosome BEL1 with a first rim on a mottled inherited core and a euhedral Ov2. **l** Zircon from leucosome BEL1 with a bright detrital core and three distinct overgrowths. Ov1 is very thin in this grain, but could be dated in a number of other grains (see **k**). The ages of Ov1 in this leucosome are the same as in the country rock BEM1. **m** Zircon from BEL1 with two distinct overgrowths on an inherited core. **n** Zircon from amphibolite BEM1 with a large Ov1 on an inherited core. The light embayment on the upper edge is likely an incipient Ov2

Zircon chemistry and geochronology

VAM1 metatonalite

This biotite-amphibolite is poor in zircon and the crystals recovered are euhedral, and relatively small (50–200 μm in length). The internal structure shows CL-dark cores rich in U (>2,000 ppm, BG-Tables 1–3) with limited oscillatory or mosaic zoning. The cores are surrounded by lower U (200–600 ppm) rims with weak oscillatory zoning (Fig. 3a, b). The trace element patterns for both domains are similar but the core has higher contents and a marked negative Eu anomaly. Zircons in this metatonalite, though similar in appearance to those in the cross cutting leucosome VAL1, yield no Alpine age: the rims cluster around 285 Ma, with the cores scattering in apparent age from ~280 to 250 Ma.

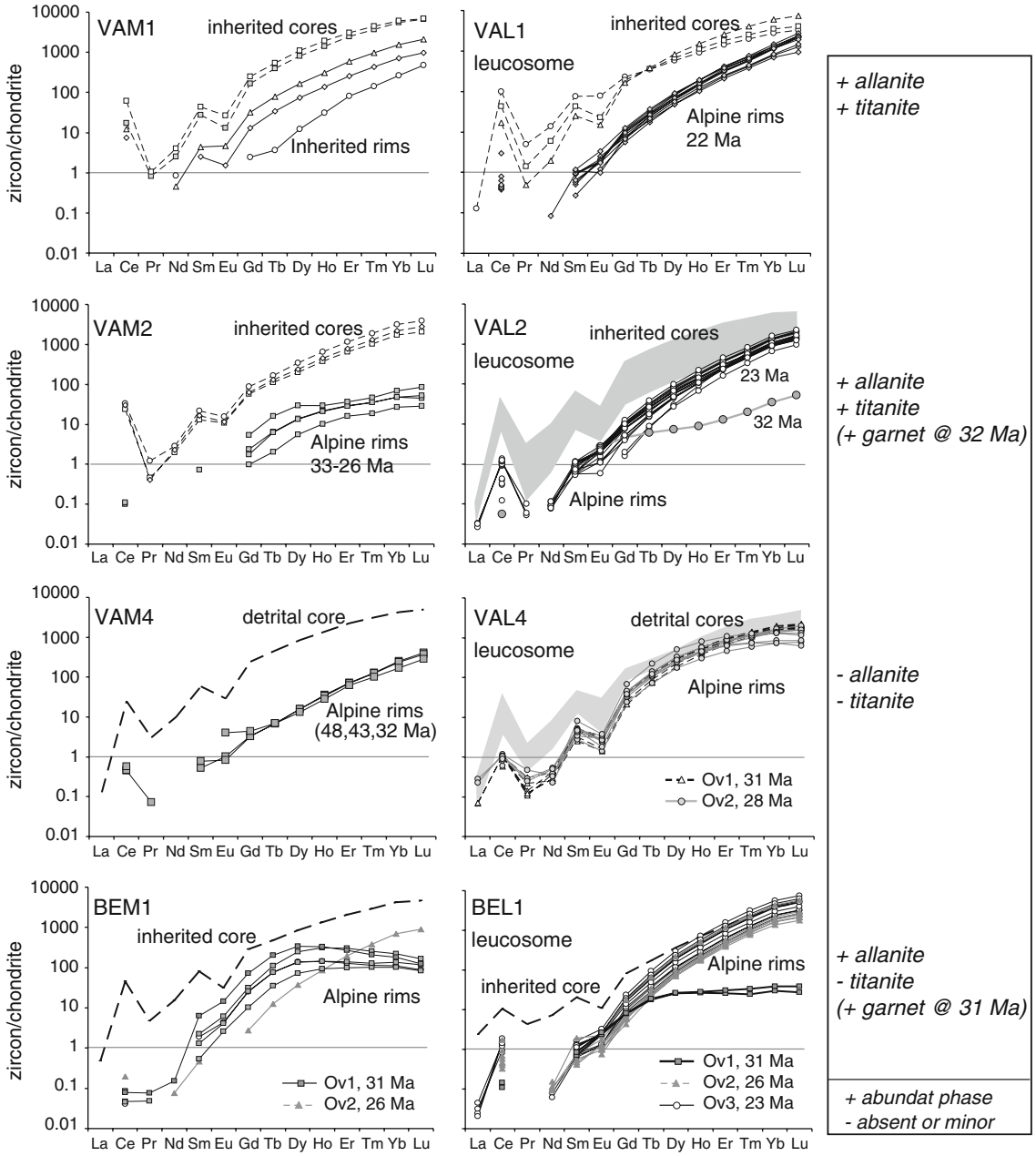

Fig. 4 REE chondrite normalized patterns for the different zircon growth domains in the investigated samples. Concentrations were measured with LA-ICPMS overlapping the SHRIMP spot wherever possible. The column on the right reports the abundance of key minerals in the Alpine assemblage. Presence of early garnet in VAL2 and BEL1 is inferred on the basis of low HREE abundance in zircon, although garnet was not observed in thin section. See text for discussion

VAL1 leucosome

In this leucosome zircons are euhedral and elongated and generally larger than in country rock VAM1. Their internal zoning consists of CL-dark, inherited cores with oscillatory or mosaic zoning, which are surrounded by one or two overgrowths with weak oscillatory–sector zoning (Fig. 3c). The overgrowths are dominant in volume and the cores are highly resorbed.

Composition and age reflect the CL zoning. The cores are rich in trace elements with a pattern enriched in HREE, and high Th/U ratio (>0.1, Figs. 4, 5a; BG-Table 1). The U–Pb age of the few cores analysed is in the range ~290–274 Ma (BG-Table 2). The overgrowths have lower trace element contents with a steep REE pattern enriched in HREE, but with concentrations being up to an order of magnitude lower than those of the cores. They lack a marked negative Eu anomaly (Eu/Eu* ~0.4). Th/U is

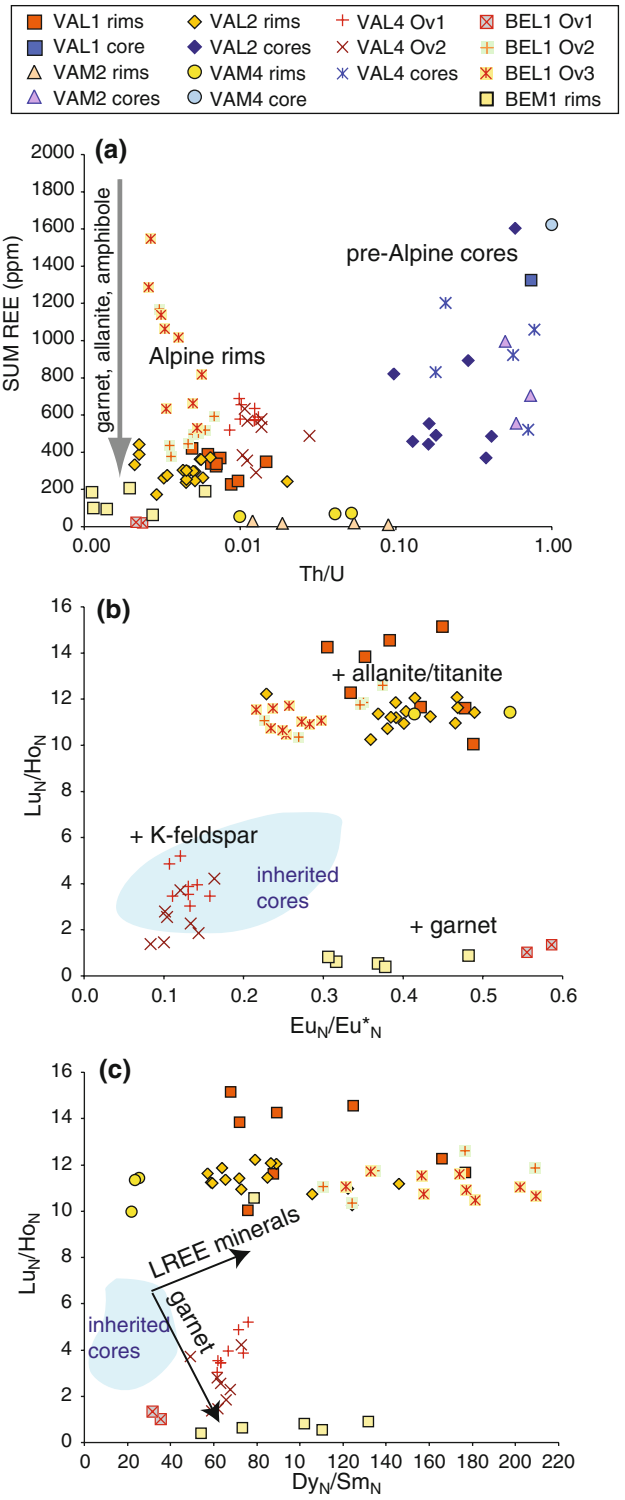

Fig. 5 Divariant plots of zircon trace element compositions. Note that elemental ratios in b) and c) are normalized to chondrite. The legend is valid for all plots. See text for discussion

systematically low at ~0.01. U–Pb analyses of overgrowths form a remarkably tight population (Figs. 6a, 7a; BG-Table 3) with an average age of 22.12 ± 0.25 Ma (MSWD 0.94).

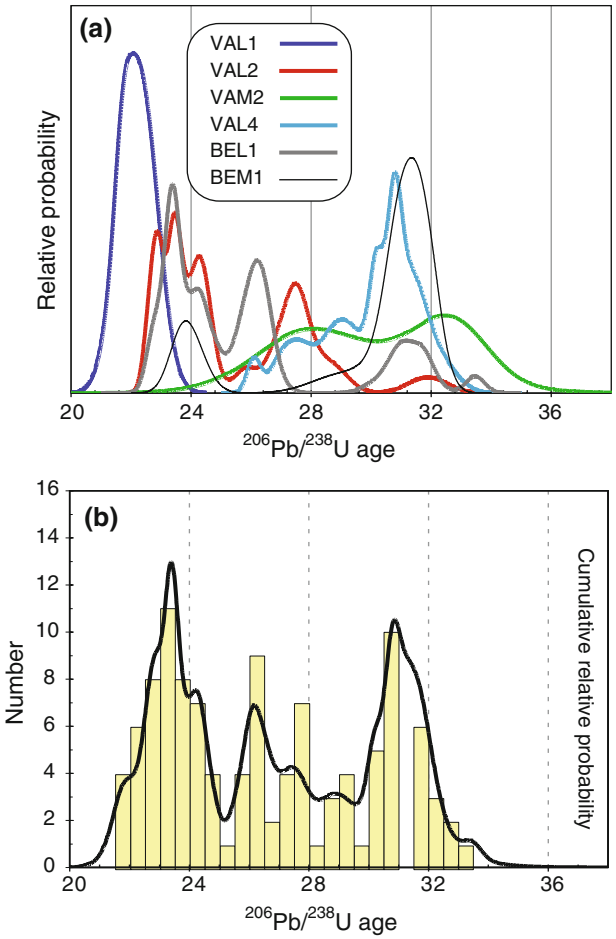

Fig. 6 Cumulative probability density plots for SHRIMP U–Pb ages of zircon. Samples are plotted with separate curves in **a** and as a cumulative curve in **b**

VAM2 metatonalite

The biotite-amphibolite contains euhedral zircon with rounded edges, denoting some resorption. The internal zoning is dominated by oscillatory cores that may display more than one growth episode (Fig. 3d). The inherited cores have trace element compositions typical of magmatic zircon: medium Th/U and a steep REE pattern with marked negative Eu anomaly (Fig. 4). Ages are around 290 Ma with some analytical scatter (BG-Table 2).

In a few crystals, the core is surrounded by an unzoned rim (Fig. 3d), which is chemically distinct having very low contents of U and Th (Th/U < 0.05, BG-Table 1) and other trace elements. The M- to HREEs are a factor of 50 lower than those of the magmatic cores, whereas M-LREE are mainly below detection limit (Fig. 4). The age of the rims scatter between ~32 and 28 Ma (Fig. 6a), with an intercept age of 31.2 ± 2.5 Ma for which an MSWD of 2.4 denotes scatter above analytical uncertainty (Fig. 7b). Analyses have a relatively high proportion of common Pb

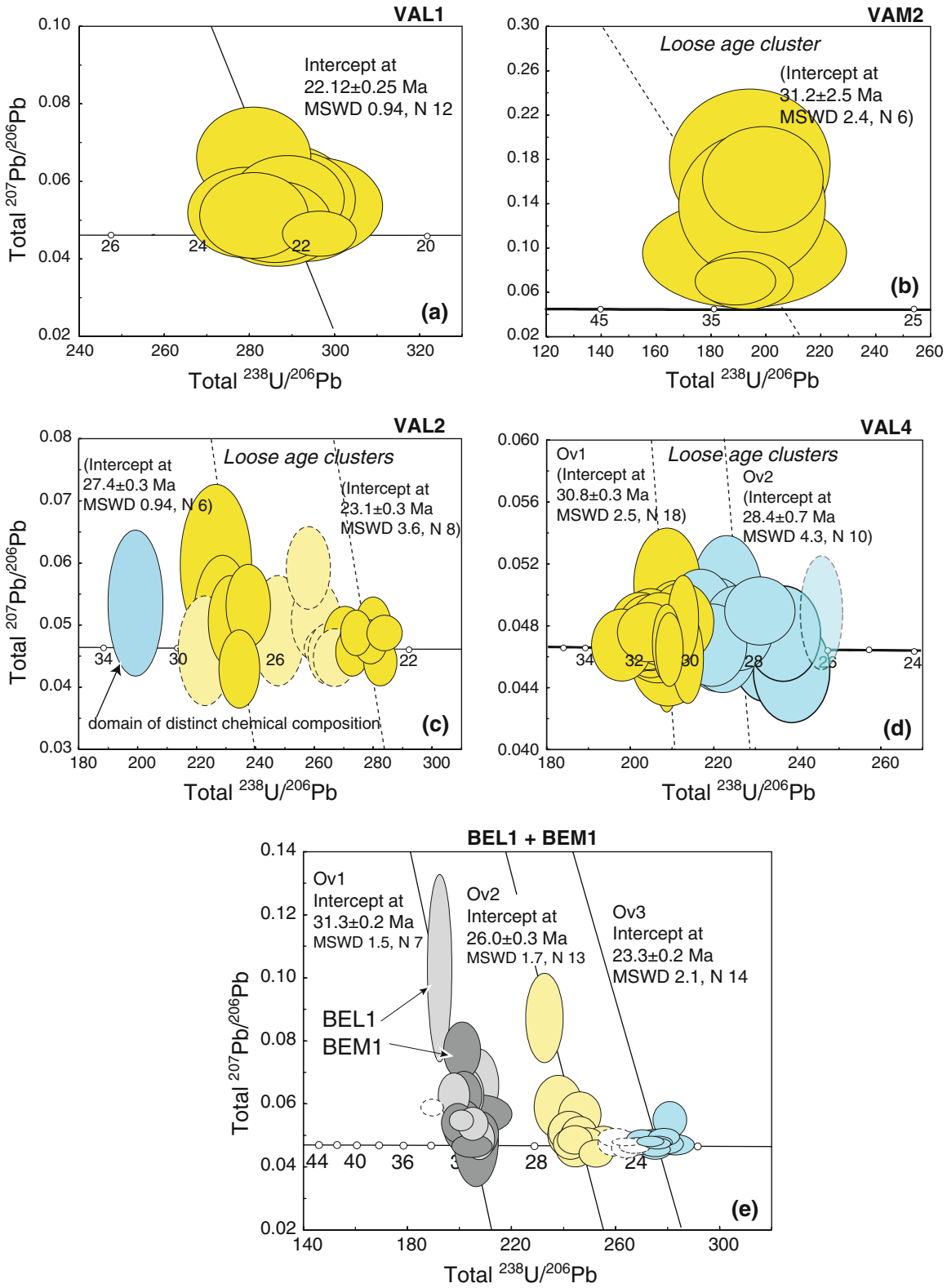

Fig. 7 Tera-Wasserburg plots for U–Pb isotopic ratios uncorrected for common Pb. Intercept ages given in *brackets* indicate "loose age groups" for which the data scatter above analytical uncertainty. *Dotted ellipses* are not used for age calculation. See Fig. 3 for zircon textures and text for discussion

(3–16%) due to the very low U (<30 ppm) and thus radiogenic Pb content (BG-Table 3).

VAL2 leucosome

In leucosome VAL2, zircons are large, euhedral and show a complex core-rim zoning. The cores display mainly oscillatory zoning and still preserve a prismatic habit (Fig. 3e), but variations with CL-dark and mosaic zoning are occasionally present. The oscillatory-zoned cores have a typical magmatic composition rich in trace elements. With one exception, ages are between 299 and 290 Ma (BG-Table 2).

In most grains, the core is overgrown by a weakly zoned or unzoned rim, which is particularly large at the crystal tips (Fig. 3e, f). The zircon rims are poor in U, Th (Th/U 0.006–0.002) and other trace elements with higher HREE and thus a steep REE pattern (Fig. 4). As in other Alpine zircon rims, the negative Eu anomaly is minor. Ages of these rims range from 31.9 to 22.6 Ma (22 analyses, Fig. 6a), with a disperse cluster at 23.1 ± 0.3 Ma (MSWD 3.6, N 8) and a better defined peak at 27.4 ± 0.3 Ma (MSWD 0.94, N 6, Fig. 7b). The scatter of ages correlates with a mild variation in chemistry, with the ~23 Ma zircon rims forming a homogeneous chemical group. Variations in Alpine age are observed within single crystals, where the internal part of a rim is always older than the external part. Such age variations can occur within domains with continuous zoning (Fig. 3f). In one single grain, a significantly older overgrowth (31.9 ± 0.6 Ma, 1 sigma) is found internally to the ~28 Ma zircon rim (Fig. 3e). This older overgrowth is chemically distinct from all others in this sample and similar in zoning and composition to the ~30 Ma overgrowths in the country rock.

VAM4 metasediment

This metasediment yielded relatively few zircons, which are dominated by cores with variable zoning, as expected for detrital grains. The REE composition is typical of magmatic zircon (Fig. 4). Two analyses on cores with different Th/U ratio yielded ages of ~584 and 443 Ma (BG-Table 2).

A number of crystals have a thin unzoned rim, which only in a couple of cases were large enough for analysis (Fig. 3g). They have a distinct composition with low trace element contents, low Th/U and steep REE patterns with LREE below detection limit (Fig. 4). Three U–Pb analyses on rims without overlapping with cores, yielded dates at 48, 43 and 32 Ma (BG-Table 3), which however cannot be assessed for concordance and thus offer little insight in the age of the rims. The data may suggest an Alpine age, possibly at the older end of the spectrum obtained in other samples.

VAL4 leucosome

In this large, partly cross-cutting leucosome, zircon grains are euhedral and composed of cores and overgrowths (Fig. 3h–j). The cores show variable zoning patterns, from oscillatory to unzoned and CL-dark, and are often corroded and fractured. The composition of such cores is variable in Th and U, but remarkably similar in REE. Ages are highly variable ranging from 2799 ± 21 Ma (discordant, $^{207}Pb/^{206}Pb$ age given) to 510 ± 8 Ma (concordant $^{206}Pb/^{238}U$ age, BG-Table 2).

In most grains, the core is surrounded by one or two overgrowth lacking distinct zoning. The internal overgrowth is darker in CL than the external one, thus allowing cross-cutting relationships to be seen (Fig. 3h–j). Both overgrowths have high U (>600 ppm) and low Th (<20 ppm) and similar trace element contents and patterns, with a steep HREE enrichment and a marked negative Eu anomaly. The REE composition of the overgrowths is only marginally different from the cores (slightly lower concentrations in L-MREE, Fig. 4). Although similar in composition, the two overgrowths have distinct ages with the internal overgrowths between 32.5 and 30.1 Ma (30.8 ± 0.3 Ma, MSWD 2.5) and the external overgrowth between 29.6 and 26.1 Ma (average with one exclusion 28.4 ± 0.7 Ma, MSWD 4.3, Fig. 7d). Both populations show scatter above analytical uncertainty.

BEM 1 metatonalite

In this banded biotite-amphibolite, zircons are large, euhedral and elongated prisms (main dimension 200–400 μm) with well-developed oscillatory zoning. One single core was dated (311 ± 3 Ma, concordant $^{206}Pb/^{238}U$ age, BG-Table 2) to confirm the Carboniferous-Permian age found in the associated leucosome BEL1. The zircon trace element composition reflects a magmatic origin.

A few of the larger zircon grains have an unzoned or weakly zoned overgrowth (Ov1, Fig. 3n) with a composition significantly different from the core, i.e. low Th/U and low trace element content. The REE pattern shows a weak negative Eu anomaly and is depleted in LREE, with a flat HREE pattern at 100–200 times chondrite, significantly lower than the cores (Fig. 4). These overgrowths yield a consistent age at 31.4 ± 0.3 Ma (Fig. 7e). In a couple of grains a second overgrowth (Ov2) with brighter CL emission is present, occasionally forming embayments suggestive of zircon dissolution before growth of Ov2. The REE composition of this second overgrowth is distinct from the 31 Ma overgrowths in that it has a very steep pattern with LREE below detection and strong enrichment in HREE (Lu/Gd 330, Figs. 4, 5). A few analyses on this external overgrowth yield ages from 29.0

to 23.7 Ma (BG-Table 3), which scatter did not allow calculation of an average age.

BEL1 leucosome

This leucosome intruding along the axial plane of folds is rich in zircons, which are euhedral, elongated and clear. Their internal structure is particularly complex with cores and three distinct overgrowths (Fig. 3k–m). The cores are generally rounded, often fractured and show embayments indicating resorption. The cores display a variety of zoning patterns and ages with concordant (>89%) data at ~718, 596 and 304 Ma (BG-Table 2).

The cores are often wrapped by a thin (<10 μm) CL-dark zone on which euhedral overgrowths form. The most internal overgrowth (Ov1), which is found in a minority of grains, has irregular boundaries with the core and no internal zoning (Fig. 3k, l). It has variable Th and U contents, but restricted Th/U around 0.002. It is poor in REE and has a flat HREE pattern similar to the overgrowth in the country rock BEM1 (Figs. 4, 5). Its age also matches the BEM1 overgrowths at 31.3 ± 0.3 Ma. When the two samples are combined a cumulative age of 31.3 ± 0.2 Ma is obtained (MSWD 1.1, Fig. 7e).

The intermediate overgrowth (Ov2) is present in most grains, displays cross cutting relationships with Ov1 and is more significant in volume (Fig. 3k–m). It shows higher CL emission and no significant zoning. It has intermediate U content and low Th (Th/U 0.002–0.006), and a steep REE pattern with a weak negative Eu anomaly. Ages form a tight cluster at 26.0 ± 0.3 Ma (Fig. 7e).

A third and volumetrically important overgrowth (Ov3) can be distinguished from Ov2 mainly because it is CL-darker and shows weak sector zoning (Fig. 3l, m). Compositionally it is similar to Ov2 with a steep REE pattern, with only slightly higher trace elements, but significantly higher U (>1,000 ppm). SHRIMP analyses of the third overgrowth yield ages between 24.7 and 22.7 Ma with a major cluster at 23.3 ± 0.2 Ma (Fig. 7e).

Ti-in-zircon thermometry

Titanium was routinely measured during LA-ICPMS trace element analyses. Accuracy was monitored with a secondary standard (BCR glass) and was within 2–10%. All the zircon Alpine overgrowths have remarkably similar but low Ti commonly between 1 and 3 ppm. All the samples contain quartz, hence the activity of SiO_2 is buffered at unity. However, the samples do contain titanite and no rutile, hence the activity of TiO_2 is estimated at ~0.5, forcing an upward correction of 50°C on the temperature (Watson and Harrison 2005). The temperatures calculated in this way are mostly between 620 and 700°C (Table 1), which are in good agreement with the estimated temperature of fluid-induced melting in this area (Burri et al. 2005; Berger et al. 2008). We therefore interpret the calculated temperature of 620–700°C as the temperature at which the Alpine zircon overgrowths formed. Notably, these temperatures correspond to the T-peak obtained for the regional Barrovian cycle across the migmatite belt and adjacent units (Todd and Engi 1997).

Inherited Early Permian cores in metatonalites and associated leucosomes yielded temperatures between 690 and 830°C (corrected for a_{TiO2} ~ 0.5, because there are relics of magmatic titanite), which is higher than the temperature calculated from the Alpine anatectic rims. Such temperatures clearly underestimate the liquidus temperature of tonalites, but rather represent Zr saturation temperatures in the cooling melt (Hiess et al. 2008).

Mineral inclusions

The Alpine zircon overgrowths contain a limited number of inclusions, though most of the large overgrowths are inclusion free. The few inclusions found are of minerals that are common in the matrix, like apatite, quartz (VAL1), K-feldspar, biotite (VAL4), allanite and amphibole (BEL1). The most relevant inclusion was a glass inclusion of granitic composition (Al_2O_3 11% and SiO_2 63%) found in a 31 Ma old rim in sample BEM1. This supports the conclusion that the rim formed during anatexis. Additionally, fractures cutting across zircon overgrowths are filled with amphibolite-facies minerals such as high-Ti biotite and K-feldspar. Magmatic or detrital cores have inclusions of quartz, feldspars, biotite and, in the metatonalites, allanite.

Discussion

Age interpretation

The U–Pb analyses reveal three overall age brackets: pre-Variscan >350 Ma, Variscan ~300–275 Ma and Alpine 32–22 Ma.

In metasediment VAM4, pre-Alpine zircon grains and their cores have a shape (often rounded), CL pattern (variable from grain to grain) and variable age indicating a *detrital* origin. Similar zircon cores are found in the cross cutting leucosome VAL4. It was not the purpose of this study to investigate the age and provenance of sediments; the few core ages obtained merely confirm the expected pre-Variscan deposition. Sample BEM1 also contains pre-Variscan zircon cores with variable zoning, which are

interpreted as inherited grains present in the original tonalite/granodiorite.

Metatonalites (VAM1, VAM2 and BEM1) and associated leucosomes contain *inherited* magmatic zircon crystals or cores. Their shape (often euhedral), CL pattern (oscillatory/sector similar over the entire population), compositions (Th/U > 0.1, steep REE pattern with a marked negative Eu-anomaly) and age (mostly around 300–275 Ma) suggest magmatic crystallization dating tonalite intrusion. The late-Variscan intrusion age confirms that these rocks underwent only Alpine metamorphism and that loss of Pb from the zircons was not significant during metamorphism. A few high-U cores, particularly in sample VAM1, yielded scattered ages younger than 275 Ma. The mosaic zoning and the porosity observed in these cores suggest fluid alteration or metamictization related to the high U content (Nasdala et al. 2009), which would be responsible for Pb loss. Such features were never observed in the Alpine zircons.

The Alpine overgrowths on detrital or inherited cores have common features in all samples: they display euhedral shape, better developed in the leucosome and in the younger overgrowths, internal zoning is weak, Th/U low (<0.06), the REE composition is distinct from the cores (except in VAL4), and the overgrowths yield remarkably uniform formation temperatures between 620 and 700°C. As will be outlined in detail in the next section, these features argue for a common formation of the overgrowths during fluid-induced partial melting.

An anatectic origin is compelling for the large majority of overgrowths. However, for the earliest Alpine zircon overgrowths there is a possibility that they formed at sub-solidus conditions. It has been documented that in prograde sequences metamorphic zircon formation occurs only at or after melting (Vavra et al. 1996; Rubatto et al. 2001). However, it is also true that sub-solidus zircon formation in the form of recrystallization and/or dissolution precipitation by fluids occurs in a variety of instances (e.g. Rubatto et al. 1999; Williams 2001; Tomaschek et al. 2003; Dempster et al. 2008). Sub-solidus zircon growth may be distinguished from anatectic zircon on the basis of its irregular shape, micro-size porosity or mineral inclusions. It has also been proposed, and extensively confirmed that low trace element content is characteristic of sub-solidus zircon (Hoskin and Black 2000). In the investigated samples, sub-solidus growth thus cannot be completely excluded for the few small, irregular, and low-REE Alpine rims that are found in the country rocks. Possible sub-solidus zircon are the two rims in VAM4 that returned ages of 43 and 48 Ma, and the 28–32 Ma rims in VAM2, which have peculiarly low trace element content with nearly flat REE pattern (Fig. 4). Notably, Ti-thermometry for these potentially sub-solidus zircons returns temperatures similar to the unambiguously anatectic overgrowths.

Zircon chemistry as indictor of metamorphic assemblage

The systematic study of zircon in a number of leucosome–country rock pairs allows investigating which chemical parameters in the zircon chemistry may be indicative of certain conditions.

Alpine overgrowths are systematically low in Th/U < 0.1 (0.06–0.001, Fig. 5a) regardless of the variable amounts of U (4–4,500 ppm) and Th (0.1–20 ppm). Detrital and inherited cores of magmatic origin always have Th/U > 0.1. In these rock types, thus, the low Th/U values serve as indicators of metamorphic origin. This criterion, accepted by the geochronological community, has been found invalid in a number of situations, mainly in high (Schaltegger et al. 1999) and very high-temperature granulites (Möller et al. 2002; Hokada and Harley 2004). In the studied samples, the presence of a Th-rich phase such as allanite, which has high Th/U, is likely to be responsible for the low Th/U in the zircon overgrowths. At the relatively low temperature experienced during fluid-induced melting, LREE solubility is low in anatectic melts (Montel 1993) and thus allanite is present. At higher temperatures, the enhanced solubility of LREE in the melt may cause undersaturation, i.e. Th-rich phases such as allanite or monazite may be dissolved, in turn leaving zircon as the main reservoir for Th.

The negative Eu anomaly in the zircon overgrowths varies from minimal to moderate (Eu/Eu* 0.6–0.1), and in many cases is less pronounced than in the magmatic cores (Fig. 5b; BG-Table 1). Negative Eu anomaly in zircon has often been ascribed to the co-crystallization or sub-solidus equilibrium of a feldspar phase, which sequestrates Eu (Hinton and Upton 1991; Schaltegger et al. 1999; Rubatto 2002). Plagioclase is present in all the samples investigated, but the negative Eu anomaly is often weaker than expected. This can be attributed to two main processes. (1) In the leucosomes, zircon formation may occur before melt, and thus plagioclase, crystallization. The melt is not expected to have a significant Eu anomaly and thus also zircon in equilibrium with such a melt will lack a Eu anomaly. A similar feature has been observed in peritectic garnet that formed during fluid-assisted melting in metabasic rocks in Central Australia (Storkey et al. 2005). While this process is likely to be dominant in the leucosomes, it cannot fully explain the small negative anomaly of the zircon overgrowths in the melanosomes. (2) Metamorphic plagioclase has overall significantly lower REE than magmatic plagioclase (Gregory et al. 2009). As a consequence, REE mass balance for sample VAM1 revealed that plagioclase hosts less than 5% of the total Eu in the rock (Gregory 2008) and thus cannot impose a strong negative Eu-anomaly on coexisting minerals. Moreover, in

the biotite amphibolites, former magmatic K-feldspar with a strong positive anomaly was likely transformed to metamorphic biotite with insignificant Eu anomaly, thus liberating Eu.

Two types of zircon overgrowths can be distinguished based on their REE composition (Figs. 4, 5; BG-Table 1). The youngest (22–26 Ma, sample VAL1, VAL2, BEL1) and often more abundant overgrowths have a steep to very steep HREE pattern (Lu/Ho ~10–16) with variable amounts of total REE from very low (ΣREE ~10) to values similar to magmatic zircon (ΣREE ~1,500 ppm). These zircon overgrowths are also heavily depleted in LREE (Dy/Sm > 100, e.g. BEL1 and VAL1), significantly more than the inherited magmatic cores (Fig. 5c). These samples correspond to localities where the country rock and/or the leucosome are particularly rich in allanite that sequestrates LREE (Gregory et al. 2007) and titanite that is the main host for MREE (Gregory 2008). For example, leucosome BEL1 is particularly rich in allanite and its zircons have the most depleted LREE patterns. The allanite and titanite present during melting are thus responsible for retaining the LREE and MREE that are depleted in the coexisting zircon overgrowths.

Most of the older overgrowths (31–28 Ma in samples VAM2, VAL4, BEM1 and BEL1) have a flat HREE pattern with Lu/Ho of 0–6, with the lowest values in sample BEL1. Such low-HREE zircons are unexpected given the mineral assemblage present in the rocks (Table 1). Particularly, nearly flat HREE patterns in zircon are commonly attributed to the presence of garnet, which sequestrated HREE (Rubatto 2002). Titanite and amphibole may also contain significant HREE, but they would equally or even stronger lower the MREE, as documented in other zircon overgrowths. Garnet was not observed in these samples (with the exception of minor resorbed garnet in VAM4 and VAL4), but has been described elsewhere in Bellinzona and Val Arbedo migmatites (Berger et al. 2008). Additionally, in the metamorphic grid calculated by Berger et al. (2008) for an average migmatite composition with varying Ca content, garnet is present over most compositions at 650–750°C and 0.8 GPa (see also Gardien et al. 2000). It is thus suggested that, even though garnet might not be preserved, it was likely stable in some of the samples when the early, low-HREE zircon formed, probably during an early higher pressure metamorphic stage. For this composition, and at this temperature, melting can in fact occur up to pressure of at least 1.1 GPa (Burri et al. 2005).

The combined effects of major and accessory minerals buffering the melt can be seen in the differences in the composition of zircon in rocks derived from sedimentary (VAL4) and magmatic protoliths (VAL1, VAL2 and BEL1). The metatonalites are rich in LREE-MREE minerals such as allanite and titanite, respectively. As a consequence, zircon rims in these leucosomes have steeper REE patterns. On the other hand, leucosome VAL4 located within metasediments contains neither allanite nor titanite, and its Alpine zircons are relatively rich in L-MREE, and remarkably similar in REE composition to the detrital (likely magmatic) cores (Figs. 4, 5). Notably the REE signature of zircon overgrowths formed in leucosomes were feldspars crystallized later than zircon, and where garnet was present in the source (BEL 1), is remarkably similar to that of eclogite-facies zircon (Rubatto 2002). This is a reminder that zircon trace element signatures are not necessarily unique and indicative of a metamorphic facies, but simply reflect the local assemblage.

Fluid-assisted melting over 10 My

The spread of ages between ~32 and 22 Ma in the zircon overgrowths is considered geologically significant and the reflection of prolonged melting (see discussion below). The possibility of partial Pb loss from initial 32 Ma zircons to produce a 32–22 Ma spread is deemed impossible due to: (1) the relatively low *T* of metamorphism, well below diffusion of Pb in zircon; (2) the lack of a mylonitic foliation in the samples or crystal-plastic deformation in the zircon capable of enhancing Pb loss (cf. Reddy et al. 2006); (3) the lack of hydrothermal alteration or low *T* recrystallization in the major rock assemblage or in the zircon themselves (cf. Tomaschek et al. 2003; Rubatto et al. 2008); (4) the young age of the zircon which does not allow for accumulation of radiation damage; (5) the preservation of inherited intrusion ages in most zircon cores, and (6) the presence of texturally different overgrowths yielding distinct ages (see BEL 1 and VAL4) which is incompatible with a Pb loss hypothesis.

Three types of ages were obtained for the Alpine overgrowths, as summarized in Fig. 8:

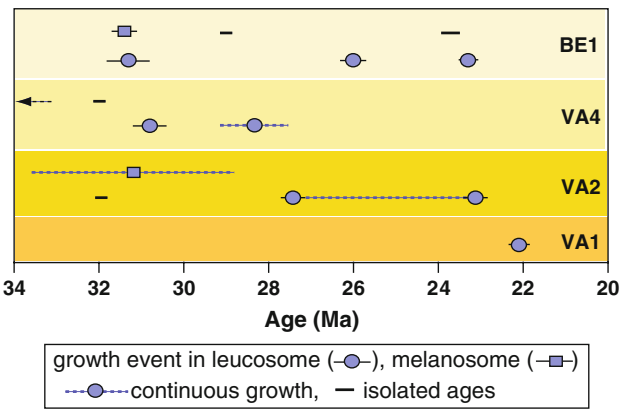

Fig. 8 Summary of zircon U–Pb ages indicating 10 My of fluid-assisted partial melting. Data are from Table 1. See text for discussion

(1) Ages defined by a tight cluster of statistically uniform analyses (MSWD of 1–2) that correspond to texturally and chemically similar zircon domains. This is the case for the single zircon overgrowth in leucosome VAL1 or the three distinct overgrowths in BEL1 (Fig. 7b). Such ages are taken to represent a short-lived event of zircon growth upon rapid melt crystallization or whenever Zr saturation is achieved in a melt pod.

(2) Loose age groups or a continuum of ages, which scatter well above analytical uncertainty and correspond to apparently similar and texturally continuous domains. Good examples are the overgrowths in VAL2 (Fig. 3f), which despite their chemical homogeneity (Fig. 4d) yielded ages between 28.8 ± 0.5 and 22.6 ± 0.2 Ma with loose peaks at (23 ± 0.3, MSWD 3 and 27.4 ± 0.3 Ma MSWD 1). Similar cases are zircon overgrowth in VAM2 and overgrowth 1 in VAL4 (Table 1; Fig. 6a). Such data are reported in brackets in Table 1 and rendered as dotted line in Fig. 8. At first sight, these features could be explained by partial Pb loss at ~23 Ma of zircon that formed at ~29 Ma. This scenario is excluded based on the arguments listed at the beginning of this section. Because such age variations are found even within single crystals (Fig. 3b), we interpret such populations to indicate zircon growth at roughly constant conditions over a period of time. Notably, age variations within single crystals always follow textural criteria, i.e. the external part of the zircon is the youngest. A possible scenario for the formation of such zircon is frequent remelting of the same leucosome under repeated fluid influx and without changing the mineral assemblage.

(3) Isolated ages on zircon rims that may show similar features. An example is amphibolite VAM4 (Fig. 3g), where three analyses on apparently similar rims returned significantly different ages at ~48, 43 and 32 Ma. Isolated ages were also measured in the young rims of BEM1. In these cases limited geological information can be gained, and isolated ages are largely excluded from the following discussion.

Within a single sample there may be more than one zircon growth episode. The three distinct zircon overgrowths in sample BEL1, the ages of which span over 10 My (Fig. 7b), are a striking example. The uniform Ti content of the overgrowths (Table 1) indicates that the three melting events occurred at a restricted temperature interval. The identical REE composition of the two youngest overgrowths (Fig. 4) also argue for an essentially identical buffering paragenesis at ~26 and 23 Ma. Additionally, Berger et al. (2008) concluded that variations in mineral compositions within single samples in the migmatite belt are indicative of limited changes in pressure (0.1 GPa) and temperature (90°C) during melting. Thus we conclude that the repeated melting events occurred within a single Barrovian metamorphic cycle at roughly constant temperature.

In three of the investigated leucosome–country rock pairs, Alpine zircon overgrowths were found in the country rock. These overgrowths are rare compared to what is found in the associated leucosome, and mostly record the oldest Alpine events (30 Ma or older). Such older ages are also found in the leucosome together with younger overgrowths. It can thus be concluded that in the amphibolites limited zircon formation occurred for the first time when zircon-forming conditions were reached (either melting or sub-solidus dissolution-precipitation), but then no further growth occurred. When further melts were produced, zircon growth concentrated in the leucosome, whereas in the country rock zircon may have undergone dissolution.

Short-lived zircon growth mainly occurs in the leucosomes, whereas isolated or protracted ages are more common in the country rocks. This suggests that whenever melt was removed from its source, even over short distances, and migrated into a leucosome, zircon crystallization was rapid. Rapid crystallization of the melt was likely favoured by chemical gradients, notably activity of H_2O. The composition of the leucosomes in this system is that of a eutectic melt, and thus particularly suitable for (re)melting if additional fluid is made available. In this scenario new zircon can form over an extended period of time by dissolution-precipitation in a continuingly remelting anatectic pocket (Fig. 9).

These constraints define a scenario in which the Central Alps migmatites were kept at nearly constant conditions (T of 620–700°C) between ~32 and 22 Ma, with limited pressure and temperature variations. Over this period melting occurred intermittently and repeatedly within any sample, whenever fluids entered the system. This scenario is schematically summarized in Fig. 9, where initial melting and zircon growth occurs in amphibolites and leucosomes, but successive melting is concentrated in the leucosome because of its favourable composition. The local composition of the rocks and localized nature of the fluids means that melting occurred at different times in samples a few meters apart (see VAL2 and VAL1).

Timing of fluid-assisted versus hydrate-breakdown melting

Previous geochronological investigations of migmatite and crustal melting dealt with terranes where hydrate-breakdown melting is by far the dominant process (Vavra et al. 1996; Williams et al. 1996; Schaltegger et al. 1999; Jung

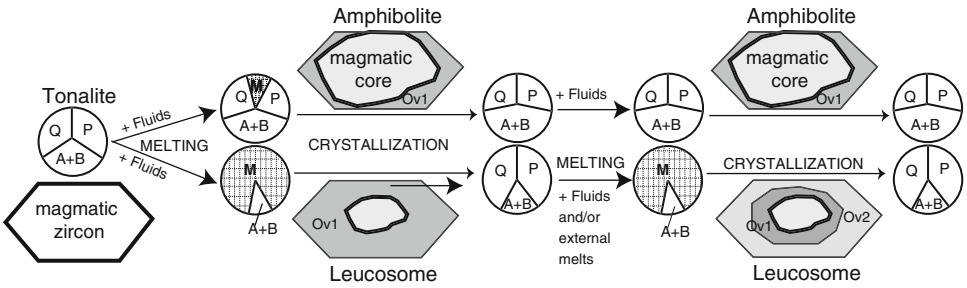

Fig. 9 Schematic representation of melting and zircon growth during fluid-assisted melting in the investigated samples. The *pie* diagrams indicate the relative amount of phases (*Q* quartz, *P* plagioclase, *A* + *B* amphibole and biotite, *M* melt). Melting is limited by the external influx of fluids and is more efficient in the leucosomes because of their favourable composition. Successive remelting of leucosomes causes partial dissolution-precipitation of existing zircon and formation of successive overgrowths. The model is further discussed in the text

and Mezger 2001; Rubatto et al. 2001; Montero et al. 2004). The data presented here, even though limited to a single terrane, allow constraining the timing and the behaviour of zircon during fluid-assisted melting.

It has been extensively documented that during hydrate-breakdown melting the degree of zircon growth and, thus, likely melt production is dependent on the chemical composition of the rock. Metapelites are richer in hydrous minerals, thus produce more melt, and in turn more anatectic zircon than metapsammites at equal conditions (Vavra et al. 1996; Rubatto et al. 2001). In the Central Alps, both metatonalites and metasediments have similarly abundant anatectic zircon overgrowths. This apparent lack of chemical bias in zircon production is to be expected for two reasons. (1) Melting is regulated by external fluid influx and not internally by the paragenesis. (2) The composition of low *T* (eutectic) melts is similar in metatonalites and metasediments. Therefore, at similar melt compositions and amounts of fluid, similar anatectic zircon production will be present in different rocks during fluid-induced melting.

In regional migmatites derived from hydrate-breakdown melting reactions, it is often observed that anatectic zircon growth is concentrated in the leucosome rather than in the restite or mesosome, where inherited zircon grains are instead preserved. The same observation is true for the migmatites of the Central Alps. This confirms that zircon growth is induced by the melt via dissolution-reprecipitation (e.g. Vavra et al. 1996), rather than being related to breakdown reactions of other Zr-bearing minerals (cf. Bingen et al. 2001; Degeling et al. 2001).

Similarly to the case presented here, extended periods of partial melting (over >10 Ma) have been documented in migmatites where hydrate-breakdown melting is dominant (Vavra et al. 1996; Williams et al. 1996; Jung and Mezger 2001; Rubatto et al. 2001; Montero et al. 2004). In each case investigated, the duration of melting is given by distinct ages in different leucosomes or country rocks, with zircon or monazite within each sample having one single anatectic growth stage. To our knowledge, during water-absent melting the same leucosome never records more than one zircon overgrowth. Even in migmatites where melt mobilization is considered minimal, as in the low *T* granulites of Mt Stafford, central Australia, in each sample zircon records only one melting episode (Rubatto et al. 2006). There are, however, limited reports of multiple zircon growth preserved in restites during high-temperature melting (Möller et al. 2002; Hermann and Rubatto 2003). On the other hand, in the migmatites of the Central Alps three of the studied leucosomes have zircon with multiple overgrowths. These observations suggest a difference in the way the two melting processes progress. During dehydration reactions, melting is efficient and produces leucosomes that readily crystallize zircon. The leucosomes are poor in hydrate minerals and thus are not prone to be re-melted. In these terranes, protracted melting is recorded by production of subsequent leucosome generations. In the case of low temperature, fluid-assisted melting, melt is localized in pockets wherever fluids are available. If melting conditions persist and fluids are available, melt pockets having an eutectic composition will easily be reactivated (re-melted or injected with new melts), each time producing a new episode of zircon dissolution-precipitation (Fig. 9).

Our result that leucosomes form at different times within the same rock unit has important implications for the role of melting in such migmatites. While the field observation might suggest that a large amount of partial melting occurred in these rocks, the geochronology indicates that at any given time the amount of leucosome was rather small. Hence, this type of melting is unlikely to produce large granitic bodies. In fact, the Novate-intrusion further to the East is the only kilometre-sized body of anatectic granitic melt in the Alps. Additionally, when the rheological state of deep crustal rocks is deduced from field observations of such migmatites, it is important to consider that not all

observed leucosomes were present at the same time. In particular, a recent numerical model (Faccenda et al. 2008) has shown that extensive partial melting in the deeply buried crust can be responsible for fast exhumation. Based on our findings, such a model has probably only limited application for the Central Alps as there is no evidence for a pronounced pulse of crustal melting.

Implications for Alpine Barrovian metamorphism

The Central Alps represent a typical terrane of Barrovian-type metamorphism. Isograds have been mapped showing an increase in temperature toward the migmatite zone (e.g. Todd and Engi 1997) where the investigated samples were collected. The timing of peak metamorphism in the region recording amphibolite-facies is constrained by remarkably few data. Dating of garnet and its inclusions via U–Pb, Sm–Nd and Rb–Sr returned a variety of ages from 32 to 16 Ma (Vance and O'Nions 1992). Because these isotopic measurements were dominated by inclusions and may not date garnet growth, it is unclear what the ages represent in terms of metamorphic grade. The authors discarded some of the Rb–Sr ages and concluded that peak metamorphism occurred at ~30 Ma in the north and ~27 Ma in the south of the Lepontine area, in agreement with previous K–Ar cooling ages. Zircon in migmatites and granulites in the eastern and northern part of the SSB also indicated peak of metamorphism at ~32 Ma (Gebauer 1996; Liati and Gebauer 2003).

Isotope dilution U–Pb dating of accessory minerals from syn- to post-kinematic dikes returned formation ages between 29 and 25 Ma (Romer et al. 1996; Schärer et al. 1996). In the light of the complexity of the zircons in the leucosome investigated here (see cross-cutting dike VAL4) these previous ages have to be taken with caution. Nevertheless, the 29–25 Ma dike ages have been taken to constrain the metamorphic peak at around 29 ± 1 Ma, but they also indicate that crustal melting was occurring over a period of time and toward younger ages. In fact, intrusion of a major granitic body, the Novate granite, outcropping in the Eastern part of the migmatite belt was dated at 25.1 ± 0.6 Ma (Liati et al. 2000). An additional constraint on the age of metamorphism is the intrusion of the composite Bergell pluton between 33 and 28 Ma (von Blanckenburg 1992; Oberli et al. 2004). This pluton outcrops in the Eastern part of the Central Alps and the western tail of the intrusive body is considered synchronous to anatexis (Berger et al. 1996). Therefore, considering the regional distribution of ages and the possible complication introduced by intrusion of melts coming from deeper levels of the chain (e.g. Novate granite) a 32–29 Ma age for the peak of metamorphism has been accepted by many. This interpretation discarded ages of monazite from migmatites

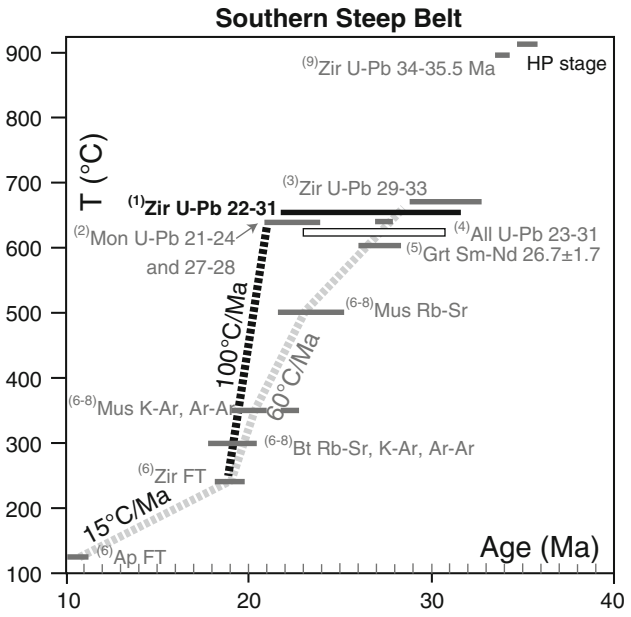

Fig. 10 Proposed cooling path for the Southern Steep Belt. The *grey* path is according to Hansmann (1996), whereas the *black* path results from this work. It should be noted that the paths combine ages from different parts of the SSB and are thus subject to extrapolations across the area. The HP stage at ~35 Ma refers to eclogites and peridotites within the amphibolite facies rocks of the SSB, north of the area investigated. Age data from: (1) this work, (2) Köppel and Grünenfelder (1975), (3) Oberli et al. (2004); von Blanckenburg (1992), (4) Gregory (2008), (5) Vance and O'Nions (1992), (6) Hurford (1986), (7) Giger (1991) as reported by Hansmann (1996), (8) Schärer et al. (1996), (9) Gebauer (1996); Hermann et al. (2006). See text for discussion

dated at 24–21 Ma (Hänny et al. 1975; Köppel and Grünenfelder 1975), which were considered anomalous or unreliable because of later resetting (e.g. Gebauer 1999).

A metamorphic peak limited to the 32–29 Ma is strongly contradicted by our study where five of the sample dated yielded ages younger than 30 Ma and as young as 22 Ma. There is compelling evidence that Alpine zircon overgrowth dated at over 31 Ma in sample BEL1 and BEM1, and all younger overgrowths in either locality are anatectic. The Alpine overgrowths are thus evidence of fluid-induced melting over a period of ~10 My (Figs. 8, 10). These new age constraints allow reinstating the 24–21 Ma ages of monazite in similar migmatites (Hänny et al. 1975; Köppel and Grünenfelder 1975). Similarly to zircon, monazite is expected to readily form during high-grade metamorphism and anatexis and preserve formation ages. The lack of ages of ~30 Ma in monazite is either a consequence of the isotope dilution method, which may fail to resolve slightly older cores, or the result of monazite dissolution and precipitation during the later episodes of melting. Additional support for long-lasting metamorphic conditions above the wet solidus comes from allanite U–Pb ages in migmatites across the migmatite belt, which show a pattern similar to

zircon, with repeated allanite formation from 31 to 23 Ma (Gregory 2008). The widespread formation of leucocratic dikes, mainly in the western part of the Southern Steep Belt, in the period of 29–25 Ma (Gebauer 1996; Romer et al. 1996; Schärer et al. 1996) and the protracted crystallization of the Bergell pluton (Oberli et al. 2004) are also in agreement with a high thermal regime during the Oligocene in this part of the chain. It should be noted that late to post kinematic ~29–25 Ma dikes found in some areas do not prevent further melting and deformation in other areas of the Southern Steep Belt. As shown by our data, melting is episodic and localized where fluids are available.

Steady-state high temperature conditions in the migmatite belt for 10 My are even more surprising because they follow a period of fast tectonics. Just 5 km North of the Bellinzona samples, slices of eclogites and HP peridotite (Alpe Arami), now hosted in crustal gneisses, were rapidly exhumed between ~35 and 32 Ma (Gebauer 1996). Moreover, about 15 km to the East, zircons from the Duria garnet peridotite formed at 34.2 ± 0.2 Ma during decompression at ca. 1.7 GPa, 820°C, and recrystallized at 32.9 ± 0.3 Ma (Hermann et al. 2006) at 0.7 GPa, 700°C. The latter conditions conform to what we propose for the formation of zircon in the migmatites and thus mark the transition from a tectonic period with fast exhumation and cooling rates to a period with much slower rates (Fig. 10).

The protraction of amphibolite-facies metamorphism and melting through the Oligocene and into the early Miocene has dramatic consequences for the cooling path (Fig. 10). For decades, classical thermochronology work proposed a monotonic cooling path for the Southern Steep Belt and the Western Bergell region (Fig. 10) from ~500 to 550°C at 25 Ma (muscovite Rb–Sr and hornblende Ar–Ar) to ~350°C at 21–18 Ma (muscovite K–Ar, biotite Rb–Sr and K–Ar) (Hurford 1986 and references therein; Hunziker et al. 1992; Hansmann 1996). Slower cooling after ~19 Ma has been inferred on the basis of fission tracks data (Hurford 1986).

Because there is compelling evidence of fluid-assisted melting at 620–700°C until 22 Ma, this cooling path has to be revised. Despite the fact that melting was intermittent and heterogeneously distributed between 32 and 22 Ma, due to limited water supply (Berger et al. 2008), the temperature must have been maintained at or close to peak, at least in the migmatite belt. This does not necessarily contradict the Sm–Nd age of Vance and O'Nions (1992), or the formation ages of isolated, late to post kinematic ~29–25 Ma dikes (Gebauer 1996; Romer et al. 1996; Schärer et al. 1996), but forces isolated pre-22 Ma cooling ages from within the migmatite belt (Hurford 1986 and references therein; Hunziker et al. 1992; Hansmann 1996) to be re-evaluated. Analytical problems associated with excess Ar or initial Sr in polymetamorphic samples might be responsible for anomalously old ages here and elsewhere within the Central Alps. Additionally, cooling might have been occurring earlier at the outskirts of the Southern Steep Belt. The zircon and monazite constraints on the persistence of high-grade conditions until at least 22–21 Ma require a dramatically faster cooling within a period of a few million years.

Muscovite and biotite ages from the migmatites are ~19–20.5 Ma (Hurford 1986 and references therein; Hunziker et al. 1992; Hansmann 1996). However, the constraints from zircon fission track dating is based on incredibly few data from within the Southern Steep Belt and none from the areas of intense migmatisation like Bellinzona or Val Arbedo (Vernon et al. 2008). The oldest zircon fission track data from the migmatite belt are at 18.9 ± 0.9 Ma (Ponte Brolla; Hurford 1986) and thus cooling to 250°C may be as young as 18 Ma. Assuming that the regional extrapolation over some 10 km is correct, a minimum cooling rate of around 100°C/Ma from the peak of metamorphism is implied. This fast cooling from peak to ~250°C is in strong contrast with slow cooling below 250°C which occurred at a rate of ~15°C/Ma, as described by zircon-apatite fission track data (Hurford 1986; Vernon et al. 2008). In fact, the late exhumation of the Central Alps in the Miocene is apparently one of the slowest within the western part of the Alps (Vernon et al. 2008).

The protracted high temperature regime in the migmatite belt does not necessarily imply that the entire Central Alps followed the same cooling path. In recent years, the SSB and its migmatites have been recognised as a tectonically distinct and complex area, and interpreted as a Tectonic Accretion Channel (Engi et al. 2001). It is possible that in other parts of the Central Alps the metamorphic peak was shorter lived or even diachronous. In particular, monazite ages (Hänny et al. 1975; Köppel and Grünenfelder 1975) suggest that the metamorphic peak was reached later in the northern part of the Central Alps, at the periphery of the regional Barrovian isograde. This is supported by recent monazite-allanite dating in the northern part, which constrain peak conditions to 18–19 Ma, followed by rapid cooling (Janots et al. 2009).

The protracted HT evolution presented here implies that the definition of a distinct metamorphic peak across the Barrovian belt is not straightforward and needs reconsideration. Within the same belt, portions remained for a long time at high grade conditions (followed by fast cooling, this work), whereas other portions underwent a more continuous heating and cooling path (e.g. Janots et al. 2009). Such dynamics are to be expected in mountain building processes, where advective and conductive heat transfer, both contributing different amounts of heat, are combined (see tectono-thermal models and their dependence on tectonic style, e.g. Roselle et al. 2002; Goffé et al. 2003; Burov and Yamato 2008).

The effect of differing contributions of advective and conductive heat transport can be also inferred from structural observations in the Lepontine Alps. The investigated migmatites have been deformed during the melting stage (see above), whereas the Barrovian overprint in the north peaked after main deformation related to nappe stacking. In the north, conductive heat transport was dominant in the last stages of evolution (Wiederkehr et al. 2008), whereas in the southern Steep Belt investigated here, advective transport of melts and solid rock masses influenced the temperature–time path.

Conclusions

The study of fluid-induced migmatites in the Alpine Barrovian belt indicates that:

(1) Melt production and associated zircon growth in such migmatites depends strongly on the amount and infiltration dynamics of fluids. As a consequence, different zircon overgrowths may not represent separated metamorphic "events", but result from repeated fluid infiltration.
(2) During the protracted high temperature history, the migmatites in the Central Alps never contained significant amounts of melts at any given time. The proportion of leucosome present in outcrops is the cumulative result of several melting episodes, commonly associated with deformation, but at roughly constant *P–T* conditions.
(3) Barrovian metamorphism in the southern central Alps has a long lasting thermal history. The new geochronological data, supported by petrological observations, require a revision of the geodynamic evolution of the Lepontine dome in the Alps, and potentially of other Barrovian terranes. This requires a more detailed knowledge of the temperature-time evolution(s) in such mid-crustal sections.

Acknowledgments The Electron Microscopy Unit at the Australian National University is thanked for access to the SEM facilities. Courtney Gregory is thanked for assisting during field work and sharing valuable information on these samples. The careful and constructive reviews of Felix Oberli and Anthi Liati are acknowledged. This work was financially supported by the ARC (DP 0556700) and the Swiss National Science Foundation (SNF 200020-109637).

References

Berger A, Rosenberg C, Schmid SM (1996) Ascent, emplacement and exhumation of the Bergell pluton within the Southern Steep Belt of the Central Alps. Schweiz Mineral Petrogr Mitt 76:357–382

Berger A, Mercolli I, Engi M (2005) The Lepontine Alps: notes accompanying the tectonic and petrographic map sheet Sopra Ceneri (1:100,000). Schweiz Mineral Petrogr Mitt 85:109–146

Berger A, Burri T, Alt-Epping P, Engi M (2008) Tectonically controlled fluid flow and water-assisted melting in the middle crust: an example from the Central Alps. Lithos 102:598–615. doi:10.1016/j.lithos.2007.07.027

Bingen B, Austrheim H, Whitehouse M (2001) Ilmenite as a source of zirconium during high-grade metamorphism? Textural evidence from the Caledonides of Western Norway and implications for zircon geochronology. J Petrol 42:355–375. doi:10.1093/petrology/42.2.355

Black LP, Kamo SL, Allen CM, Aleinikoff JM, Davis DW, Korsch RJ, Foudoulis C (2003) TEMORA 1: a new zircon standard for Phanerozoic U–Pb geochronology. Chem Geol 200:155–170. doi:10.1016/S0009-2541(03)00165-7

Brouwer FM, Burri T, Engi M, Berger A (2005) Eclogite relics in the Central Alps: PT-evolution, Lu–Hf ages and implications for formation of tectonic melange zones. Schweiz Mineral Petrogr Mitt 85:147–174

Burov E, Yamato P (2008) Continental plate collision, P-T-t-z conditions and unstable vs. stable plate dynamics: Insights from thermo-mechanical modelling. Lithos 103:178–204. doi:10.1016/j.lithos.2007.09.014

Burri T, Berger A, Engi M (2005) Tertiary migmatites in the Central Alps: regional distribution, field relations, conditions of formation and tectonic implications. Schweiz Mineral Petrogr Mitt 85:215–232

Clemens JD, Vielzeuf D (1987) Constraints on melting and magma production in the crust. Earth Planet Sci Lett 86:287–306. doi:10.1016/0012-821X(87)90227-5

Degeling H, Eggins S, Ellis DJ (2001) Zr budget for metamorphic reactions, and the formation of zircon from garnet breakdown. J Metamorph Geol 65:749–758

Dempster TJ, Hay DC, Gordon SH, Kelly NM (2008) Micro-zircon: origin and evolution during metamorphism. J Metamorph Geol 26:499–507. doi:10.1111/j.1525-1314.2008.00772.x

Eggins SM, Rudnick RL, McDonough WF (1998) The composition of peridotites and their minerals: a laser ablation ICP-MS study. Earth Planet Sci Lett 154:53–71. doi:10.1016/S0012-821X(97)00195-7

Engi M, Todd CS, Schmatz DR (1995) Tertiary metamorphic conditions in the eastern Lepontine Alps. Schweiz Mineral Petrogr Mitt 75:347–369

Engi M, Berger A, Roselle G (2001) The role of tectonic accretion channel in collisional orogeny. Gelogy 29:1143–1146. doi:10.1130/0091-7613(2001)029<1143:ROTTAC>2.0.CO;2

Faccenda M, Gerya TV, Chakraborty S (2008) Styles of post-subduction collisional orogeny: influence of convergence velocity, crustal rheology and radiogenic heat production. Lithos 103:257–287. doi:10.1016/j.lithos.2007.09.009

Gardien V, Thompson AB, Ulmer P (2000) Melting of biotite + plagioclase + quartz gneisses: the role of H_2O in the stability of amphibole. J Petrol 41:651–666. doi:10.1093/petrology/41.5.651

Gebauer D (1996) A P-T-t-path for an (ultra-)high-pressure ultramafic/mafic rock-association and its felsic country-rocks based on SHRIMP-dating of magmatic and metamorphic zircon domains. Example: Alpe Arami (Central Swiss Alps). In: Basu A, Hart SR (eds) Earth processes: reading the isotopic code. American Geophysical Union, Washington DC, pp 309–328

Gebauer D (1999) Alpine geochronology of the Central and Western Alps: new constraints for a complex geodynamic evolution. Schweiz Mineral Petrogr Mitt 79:191–208

Giger M (1991) Geochronologische und petrographische Studien an Geröllen und Sedimenten der Gonfolite-Lombarda-Gruppe

(Südschweiz und Norditalien) und ihr Vergleich mit them alpinen Hinterland, PhD Thesis University of Bern, p 227
Goffé B, Bousquet R, Henry P, Le Pichon X (2003) Effect of the chemical composition of the crust on the metamorphic evolution of orogenic wedges. J Metamorph Geol 21:123–141. doi:10.1046/j.1525-1314.2003.00422.x
Gregory CJ (2008) Allanite chemistry and U–Th–Pb geochronology. PhD Thesis, Research School of Earth Sciences. The Australian National University Canberra, p 271
Gregory C, Rubatto D, Allen C, Williams IS, Hermann J, Ireland T (2007) Allanite micro-geochronology: a LA-ICP-MS and SHRIMP U–Th–Pb study. Chem Geol 245:162–182. doi:10.1016/j.chemgeo.2007.07.029
Gregory C, Buick IS, Hermann J, Rubatto D (2009) Mineral-scale trace element and U–Th–Pb age constraints on metamorphism and melting during the Petermann Orogeny (central Australia). J Petrol 50:251–287. doi:10.1093/petrology/egn077
Hänny R, Grauert B, Soptrajanova G (1975) Paleozoic migmatites affected by high-grade tertiary metamorphism in the central Alps (Valle Bodengo, Italy)—a geochronological study. Contrib Mineral Petrol 51:173–196. doi:10.1007/BF00372078
Hansmann W (1996) Age determinations on the Tertiary Masino-Bregaglia (Bergell) intrusives (Italy, Switzerland): a review. Schweiz Mineral Petrogr Mitt 76:421–452
Hermann J, Rubatto D (2003) Relating zircon and monazite domains to garnet growth zones: age and duration of granulite facies metamorphism in the Val Malenco lower crust. J Metamorph Geol 21:833–852
Hermann J, Rubatto D, Trommsdorff V (2006) Sub-solidus Oligocene zircon formation in garnet peridotite during fast decompression and fluid infiltration (Duria, Central Alps). Mineral Petrol 88:181–206. doi:10.1007/s00710-006-0155-3
Hiess J, Nutman AP, Bennett VC, Holden P (2008) Ti-in-zircon thermometry applied to contrasting Archean metamorphic and igneous systems. Chem Geol 247:323–338. doi:10.1016/j.chemgeo.2007.10.012
Hinton RW, Upton BGJ (1991) The chemistry of zircon: variations within and between large crystals from syenite and alkali basalt xenoliths. Geochim Cosmochim Acta 55:3287–3302. doi:10.1016/0016-7037(91)90489-R
Hokada T, Harley SL (2004) Zircon growth in UHT leucosome: constraints from zircon-garnet rare earth elements (REE) relations in Napier Complex, East Antarctica. J Mineral Petrol Sci 99:180–190. doi:10.2465/jmps.99.180
Hoskin PWO, Black LP (2000) Metamorphic zircon formation by solid-state recrystallization of protolith igneous zircon. J Metamorph Geol 18:423–439. doi:10.1046/j.1525-1314.2000.00266.x
Hunziker JC (1969) Rb–Sr-Altersbetimmungen aus den Walliser Alpen, Hellglimmer- und Gesamt-gestainswerte. Eclogae Geol Helv 62:527–542
Hunziker JC, Desmond J, Hurford AJ (1992) Thirty-two years of geochronological work in the Central and Western Alps: a review on seven maps. Mémoires de Géologie (Lausanne) 13: 59 pg
Hurford AJ (1986) Cooling and uplift patterns in the Lepontine Alps, South Central Switzerland and an age of vertical movement on the Insubric fault line. Contrib Mineral Petrol 92:413–427. doi:10.1007/BF00374424
Jäger E (1973) Die alpine Orogenese im Lichte der radiometrischen Altersbestimmungen. Eclogae Geol Helv 66:11–21
Janots E, Engi M, Rubatto D, Berger A, Gregory C (2009) Metamorphic rates in collisional orogeny from in situ allanite and monazite dating. Geology 37:11–14. doi:10.1130/G25192A.1
Jung S, Mezger K (2001) Geochronology in migmatites—a Sm–Nd, U–Pb and Rb–Sr study from the Proterozoic Damara belt (Namibia): implications for polyphase development of migmatites in high-grade terranes. J Metamorph Geol 19:77–97. doi:10.1046/j.0263-4929.2000.00297.x
Kalt A, Corfu F, Wijbrans JR (2000) Time calibration of a P–T path from a Variscan high-temperature low-pressure metamorphic complex (Bayerische Wald, Germany), and the detection of inherited monazite. Contrib Mineral Petrol 138:143–163. doi:10.1007/s004100050014
Kelsey DE, Clark C, Hand M (2008) Thermobarometric modelling of zircon and monazite growth in melt-bearing systems: examples using model metapelitic and metapsammitic granulites. J Metamorph Geol 26:199–212. doi:10.1111/j.1525-1314.2007.00757.x
Köppel V, Grünenfelder M (1975) Concordant U–Pb ages of monazite and xenotime in the central Alps and the timing of high temperature Alpine metamorphism, a preliminary report. Schweiz Mineral Petrogr Mitt 55:129–132
Le Breton N, Thompson AB (1988) Fluid-absent (dehydration) melting of biotite in metapelites in the early stages of crustal anatexis. Contrib Mineral Petrol 99:226–237. doi:10.1007/BF00371463
Liati A, Gebauer D (2003) Geochronological constraints for the time of metamorphism in the Gruf Complex (Central Alps) and implications for the Adula-Cima Lunga nappe system. Schweiz Mineral Petrogr Mitt 83:159–172
Liati A, Gebauer D, Fanning M (2000) U–PbSHRIMP dating of zircon from the Novate granite (Bergell, Central Alps): evidence for Oligocene-Miocene magmatism, Jurassic/Cretaceous continental rifting and opening of the Valais trough. Schweiz Mineral Petrogr Mitt 80:305–316
Ludwig KR (2003) Isoplot/Ex version 3.0. A geochronological toolkit for Microsoft Excel. Berkeley Geochronological Centre Spec. Pub., Berkeley, p 70
Maxelon M, Mancktelow NS (2005) Three-dimensional geometry and tectonostratigraphy of the Pennine zone, Central Alps. Switz North Italy Earth Sci Rev 71:171–227
Möller A, O'Brien PJ, Kennedy A, Kröner A (2002) Polyphase zircon in ultrahigh-temperature granulites (Rogaland, SW Norway): constraints for Pb diffusion in zircon. J Metamorph Geol 20:727–740. doi:10.1046/j.1525-1314.2002.00400.x
Montel J-M (1993) A model for monazite/melt equilibrium and application to the generation of granitic magmas. Chem Geol 110:127–146. doi:10.1016/0009-2541(93)90250-M
Montero P, Bea F, Zinger TF, Scarrow JH, Molina JF, Whitehouse M (2004) 55 million years of continuous anatexis in Central Iberia: Single-zircon dating of the Pena Negra Complex. J Geol Soc London 161:255–263. doi:10.1144/0016-764903-024
Nasdala L, Kronz A, Wirth R, Váczi T, Pérez-Soba C, Willner A, Kennedy AK (2009) The phenomenon of deficient electron microprobe totals in radiation-damaged and altered zircon. Geochim Cosmochim Acta 73:1637–1650. doi:10.1016/j.gca.2008.12.010
Oberli F, Meier M, Berger A, Rosenberg CL, Giere R (2004) U–Th–Pb and 230Th/238U disequilibrium isotope systematics: precise accessory mineral chronology and melt evolution tracing in the Alpine Bergell intrusion. Geochim Cosmochim Acta 68:2543–2560. doi:10.1016/j.gca.2003.10.017
Prince C, Harris NBW, Vance D (2001) Fluid-enhanced melting during prograde metamorphism. J Geol Soc London 158:233–242
Reddy SM, Timms NE, Trimby P, Kinny PD, Buchan C, Blake K (2006) Crystal-plastic deformation of zircon: a defect in the assumption of chemical robustness. Geology 34:257–260. doi:10.1130/G22110.1
Romer RL, Schärer U, Steck A (1996) Alpine and pre-Alpine magmatism in the root-zone of the western Central Alps. Contrib Mineral Petrol 123:138–158. doi:10.1007/s004100050147

Roselle GT, Thüring M, Engi M (2002) Melonpit: a finite element code for simulating tectonic mass movement and heat flow within subduction zones. Am J Sci 302:381–409. doi:10.2475/ajs.302.5.381

Rubatto D (2002) Zircon trace element geochemistry: distribution coefficients and the link between U–Pb ages and metamorphism. Chem Geol 184:123–138. doi:10.1016/S0009-2541(01)00355-2

Rubatto D, Gebauer D, Compagnoni R (1999) Dating of eclogite-facies zircons: the age of Alpine metamorphism in the Sesia-Lanzo Zone (Western Alps). Earth Planet Sci Lett 167:141–158. doi:10.1016/S0012-821X(99)00031-X

Rubatto D, Williams IS, Buick IS (2001) Zircon and monazite response to prograde metamorphism in the Reynolds Range, central Australia. Contrib Mineral Petrol 140:458–468. doi:10.1007/PL00007673

Rubatto D, Hermann J, Buick IS (2006) Temperature and bulk composition control on the growth of monazite and zircon during low-pressure anatexis (Mount Stafford, central Australia). J Petrol 47:1973–1996. doi:10.1093/petrology/egl033

Rubatto D, Müntener O, Barnhorn A, Gregory C (2008) Dissolution-reprecipitation of zircon at low-temperature, high-pressure conditions (Lanzo Massif, Italy). Am Mineral 93:1519–1529. doi:10.2138/am.2008.2874

Schaltegger U, Fanning M, Günther D, Maurin JC, Schulmann K, Gebauer D (1999) Growth, annealing and recrystallization of zircon and preservation of monazite in high-grade metamorphism: conventional and in situ U–Pb isotope, cathodoluminescence and microchemical evidence. Contrib Mineral Petrol 134:186–201. doi:10.1007/s004100050478

Schärer U, Cosca M, Steck A, Hunziker J (1996) Termination of major ductile strike-slip shear and differential cooling along the Insubric line (Central Alps): U–Pb, Rb–Sr and 40Ar/39Ar ages of cross-cutting pegmatites. Earth Planet Sci Lett 142:331–351. doi:10.1016/0012-821X(96)00104-5

Schmid SM, Pfiffner A, Froitzheim N, Schönborn G, Kissling N (1996) Geophysical–geological transect and tectonic evolution of the Swiss-Italian Alps. Tectonics 15:1036–1064. doi:10.1029/96TC00433

Stacey JS, Kramers JD (1975) Approximation of terrestrial lead evolution by a two-stage model. Earth Planet Sci Lett 26:207–221. doi:10.1016/0012-821X(75)90088-6

Steck A, Hunziker JC (1994) The Tertiary structural and thermal evolution of the Central Alps—compressional and extensional structures in an orogenic belt. Tectonophysics 238:229–254. doi:10.1016/0040-1951(94)90058-2

Steiger RH (1964) Dating f orogenic phases in the Central Alps by K–Ar of hornblende. J Geophys Res 69:5407–5421. doi:10.1029/JZ069i024p05407

Storkey A, Hermann J, Hand M, Buick IS (2005) Using insitu trace element determinations to monitor partial melting processes in metabasites. J Petrol 46:1283–1308

Todd CS, Engi M (1997) Metamorphic field gradients in the Central Alps. J Metamorph Geol 15:513–530. doi:10.1111/j.1525-1314.1997.00038.x

Tomaschek F, Kennedy AK, Villa IM, Lagos M, Ballhaus C (2003) Zircons from Syros, Cyclades, Greece—recrystallization and mobilization of zircon during high-pressure metamorphism. J Petrol 44:1977–2002. doi:10.1093/petrology/egg067

Vance D, O'Nions RK (1992) Prograde and retrograde thermal histories from the Central Swiss Alps. Earth Planet Sci Lett 114:113–129. doi:10.1016/0012-821X(92)90155-O

Vavra G, Gebauer D, Schmidt R, Compston W (1996) Multiple zircon growth and recrystallization during polyphase Late Carboniferous to Triassic metamorphism in granulites of the Ivrea Zone (Southern Alps): an ion microprobe (SHRIMP) study. Contrib Mineral Petrol 122:337–358. doi:10.1007/s004100050132

Vernon AJ, van der Beek PA, Sinclair HD, Rahn MK (2008) Increase in late Neogene denudation of the European Alps confirmed by analysis of a fission-track thermochronology database. Earth Planet Sci Lett 270:316–329. doi:10.1016/j.epsl.2008.03.053

von Blanckenburg F (1992) Combined high-precision chronometry and geochemical tracing using accessory minerals: Applied to the Central-Alpine Bergell intrusion (central Europe). Chem Geol 100:19–40. doi:10.1016/0009-2541(92)90100-J

Watson EB, Harrison TM (2005) Zircon thermometer reveals minimum melting conditions on earliest. Earth Sci 308:841–844

White RW, Powell R, Holland TJB (2007) Progress relating to calculation of partial melting equilibria for metapelites. J Metamorph Geol 25:511–527. doi:10.1111/j.1525-1314.2007.00711.x

Wiederkehr M, Bousquet R, Schmid SM, Berger A (2008) From subduction to collision: thermal overprint of HP/LT metasediments in the north-eastern Lepontine Dome (Swiss Alps) and consequences regarding the tectono-metamorphic evolution of the Alpine orogenic wedge. Swiss J Geosci 101:S127–S155

Williams I (1998) U–Th–Pb geochronology by ion microprobe. In: McKibben MA, Shanks III WC, Ridley WI (eds) Application of microanalytical techniques to understanding mineralizing processes, vol 7. Reviews in Economic Geology, pp 1–35

Williams IS (2001) Response of detrital zircon and monazite, and their U–Pb isotopic systems, to regional metamorphism and host-rock partial melting, Cooma Complex, southeastern Australia. Aust J Earth Sci 48:557–580. doi:10.1046/j.1440-0952.2001.00883.x

Williams IS, Buick IS, Cartwright I (1996) An extended episode of early Mesoproterozoic metamorphic fluid flow in the Reynolds Range, central Australia. J Metamorph Geol 14:29–47. doi:10.1111/j.1525-1314.1996.00029.x